Sb_4 clusters: 4*d* core ionization, subsequent Auger decay, and fragmentation pathways of the Auger final states

S. Urpelainen,* A. Caló, L. Partanen, M. Huttula, S. Aksela, and H. Aksela
Department of Physical Sciences, University of Oulu, P. O. Box 3000, 90014 Oulu Finland

S. Granroth and E. Kukk
Department of Physics and Astronomy, University of Turku, FIN-20014 Turku, Finland
(Received 5 January 2009; published 10 February 2009)

The 4*d* photoelectron and satellite spectra of Sb_4 clusters are presented together with the subsequent *CVV* (core-valence-valence) Auger electron spectra. Theoretical molecular calculations were used together with semiempirical methods combining negative ion atomic calculations and existing experimental data on the noble gas xenon to predict the structure of the electron spectra. A detailed experimental analysis of the fragmentation pathways of Sb_4 after 4*d* photoionization and subsequent Auger decay was performed with the use of ion time-of-flight spectroscopy, electron-ion coincidence, and electron-ion-ion coincidence techniques. The bonding properties of the molecular orbitals have been used to qualitatively describe the observed fragmentation pathways.

DOI: 10.1103/PhysRevA.79.023201 PACS number(s): 36.40.Qv, 31.15.ae, 36.20.Kd

I. INTRODUCTION

Antimony (Sb) and its compounds are commonly used in various industries in the production of semiconductor devices, flame-retardant fabrics, paints, etc. The unique properties of InSb especially make it an extremely important compound in the electronics industry. To reach the future goals of the industry, where the manufacturing of smaller and smaller nanoscale electronic components is of interest, a vast amount of information on nanosized structures is needed. Small metal clusters provide an excellent target for studying the properties of matter between its atomic and bulk forms where the physical properties of the target are highly size dependent.

The creation of Sb_4 vapor is rather simple as Sb evaporates readily as small clusters at relatively low temperatures [1], and thus no special cluster source is needed. Nevertheless, no extensive studies on its electronic structure have been carried out. Most of the studies date back to the 1980s and the early 1990s, when mainly the atomic structure and valence shell electronic structure of Sb_2, Sb_4, and Sb_8 clusters have been analyzed theoretically and with the use of He I photoelectron spectroscopy [2–6]. Only a handful of studies on the inner shells of Sb_4 exist: For example Aksela *et al.* [7] have studied the $M_{4,5}N_{4,5}N_{4,5}$ Auger electron spectrum (AES) using electron impact excitation. The 4*d* photoionization cross section as a function of photon energy has been studied by Bréchignac *et al.* [8]. 4*d* photoionization has been studied using Al ($K\alpha$) radiation in solid state antimony by Pollak *et al.* [9]. To the best of our knowledge no studies on the Sb_4 4*d* photoelectron spectrum (PES) and the subsequent *NVV* AES have been published.

The electronic configuration of an antimony atom in its ground state is $[Kr]4d^{10}5s^25p^3$. In the first approximation each of the atoms in Sb_4 can be thought to have the 5*p* shell filled by the shared electrons from the other three atoms. Within this framework the electron configuration of antimony atoms in the Sb_4 cluster can be thought to be isoelectronic with the noble gas xenon. Consequently, the xenon atom serves as a reference for the electronic transitions in the Sb_4 cluster.

The 4*d* PES [10] and the subsequent $N_{4,5}OO$ AES together with its correlation satellite structure have been extensively studied for xenon (see, e.g., [11–13] and references therein). The Xe 5*s* PES reveals a prominent electron correlation structure (see Ref. [14] and references therein). The electron correlation of the 5*s* orbital has an effect on every electron spectrum if there are 5*s* vacancies in the initial or final state configuration. Consequently, the correlation satellite structure, which originates mainly from the final ionic state configuration interaction between the $5s^{-1}$ and $5p^{-2}5d$ configurations [13], is very intense in the $N_{4,5}O_1O_1$ and $N_{4,5}O_1O_{2,3}$ AES of Xe. In addition to the main 4*d* photolines of Xe, the $4d^{-1}(5s,5p)^{-1}nl$ shake-up satellites are also known [10,15]. The $N_{4,5}O$-*OOO* AES [16,17] following the $4d^{-1}5p^{-1}$ double photoionization have been found to overlap with the main AES of Xe.

In this work we present an experimental study of the Sb 4*d* photoionization and the following Auger decay in vapor phase Sb_4. The xenon 4*d* PES and subsequent $N_{4,5}OO$ AES with satellites have been used as a baseline for the corresponding PES and AES of Sb_4. The present results are compared with the previous findings on the valence shell electronic structure of Sb_4 and the 4*d* PES of solid antimony. Energy calculations for Sb_4 are used in assigning the experimental AES.

In the final states of the 4*d* Auger transition there are two electrons missing from the valence orbitals. If the vacancies are on bonding orbitals, the Sb_4 clusters fragment to smaller ions. In this work we also present a detailed study of the fragmentation of core ionized Sb_4 using electron-ion and electron-ion-ion coincidence techniques, which have proven to be an excellent tool for fragmentation studies (see, e.g., Refs. [19–23] and references therein).

*samuli.urpelainen@oulu.fi

The paper is organized as follows. In Sec. II the experimental conditions and equipment are described and Sec. III presents the computational methods used and the theoretical and experimental results obtained. Section III is divided into four parts: general discussion, the PES, the AES, and the fragmentation of the Sb_4 cluster. Finally, in Sec. IV a short summary about the paper is presented.

II. EXPERIMENTS

The experiments were carried out at the 1.5 GeV MAX-II synchrotron storage ring at the high-resolution soft x-ray undulator beamline I411, in the MAX laboratory (Lund, Sweden) [24]. The experimental setups were mounted on the so-called 1 m section of the beamline. For measuring the electron spectra a modified Scienta SES-100 electron analyzer mounted on an experimental station built in Oulu [25,26] was used. The coincidence events were recorded using an electron-ion coincidence apparatus consisting of the SES-100 hemispherical electron analyzer and a Wiley-McLaren type ion time-of-flight (TOF) spectrometer. A more detailed description of the coincidence setup can be found in Ref. [27]. All measurements were performed at the magic angle of 54.7° with respect to the electric field vector of the linearly polarized undulator radiation.

The Sb_4 cluster beam was produced using a commercial resistively heated oven (MBE Komponenten, model NTEZ-40) with an open pyrolytical boron nitride (PBN) crucible at temperatures around 470 °C corresponding to vapor pressure on the order of approximately 10^{-3} mbar within the heated volume [28]. At these temperatures Sb_4 is the predominant species formed in the evaporation process [1]. The background pressure of the chamber during the experiments was in the 10^{-7} mbar range.

The $4d$ photoelectron and satellite spectra were recorded at the photon energy of 90 eV, which is well above the double ionization threshold, but below the $4p$ ionization threshold located around 105 eV [29]. A constant spectrometer pass energy of 20 eV was used. The beamline exit slit and the electron energy analyzer entrance slit were chosen to be 100 μm and 0.8 mm (curved), respectively, corresponding to a photon bandwidth of 75 meV and an analyzer broadening of 66 meV. The AES was recorded at the photon energy of 90 eV and spectrometer pass energy of 20 eV. The exit slit of the monochromator and the entrance slit of the electron analyzer were 700 μm and 0.8 mm (curved), respectively. The large monochromator exit slit was chosen in order to have high photon flux at the target region for producing an intense signal of Auger electrons. Within the two-step model, the energy broadening of Auger electrons is governed by the natural lifetime of the core excited state together with the spectrometer broadening, but it is not affected by the photon bandwidth. The energy broadenings associated with the lifetime of the Xe $4d$ core holes are 104 and 111 meV for the $4d_{3/2}^{-1}$ and $4d_{5/2}^{-1}$ states, respectively [30], which are larger than the instrumental linewidths. The binding energy calibration of the $4d$ photolines was performed using the Xe $4d$ photolines [10] and the kinetic energy calibration for the AES using the Kr *MNN* Auger lines [31].

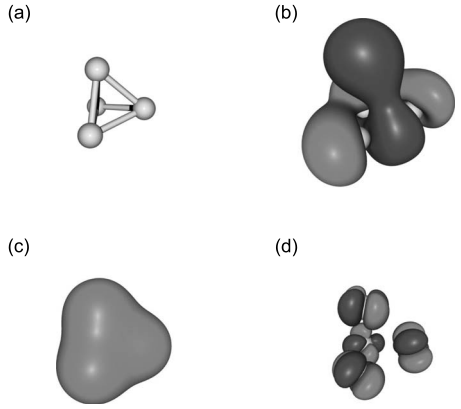

FIG. 1. Tetrahedrical structure of Sb_4 clusters and examples of isosurfaces within the T_d symmetry. (a) shows the structure of Sb_4, (b) a $6t_2$ MO, (c) a $4a_1$ MO, and (d) an (Sb $4d$)-like MO.

The coincidence experiments for both the photoelectrons and Auger electrons were performed at the photon energy of 90 eV and with a minimum aperture of the monochromator exit slit in order to maintain a good purity of the coincidence signal (see Ref. [27] and references therein). The pass energy value of the electron analyzer was set to 100 eV for the PES measurements and to 50 eV for the AES measurements, corresponding to analyzer electron energy window widths of approximately 11 and 6 eV, respectively. The electron energy analyzer entrance slit was 0.8 mm (curved). The extraction pulse voltages of the ion TOF spectrometer during the measurements were +200 and −210 V and the pulse duration 30 μs. The acceleration voltage was 1115 V.

III. RESULTS AND DISCUSSION

A. General

Theoretical calculations for molecular energy states were performed using the GAMESS software package [32,33]. The electronic structure and the ionization energies were determined using an occupation restricted multiple active space [34,35] determinant configuration interaction (CI) calculation with large-orbital–small-core potential (CRENBL effective core potential) basis set [36]. This allowed us to compute the core hole ionization and CI states without otherwise unaffordable time- and memory-consuming calculations. In the experimental conditions described in Sec. II, the evaporation from bulk antimony shows a predominant production of Sb_4 clusters. In agreement with previous studies [6], geometry optimization calculations indicated the tetrahedrical shape (see Fig. 1) as the most stable structure for Sb_4 clusters. T_d geometry has therefore been assumed for the electronic structure and ionization energy calculations. Within the T_d symmetry, the valence electronic configuration of the Sb_4 cluster is

$$(4a_1)^2(5t_2)^6(5a_1)^2(6t_2)^6(2e)^4 \quad (1)$$

corresponding to a $^1A_1$ ground state.

According to our computational results and in agreement with previous works [4], the three outermost molecular or-

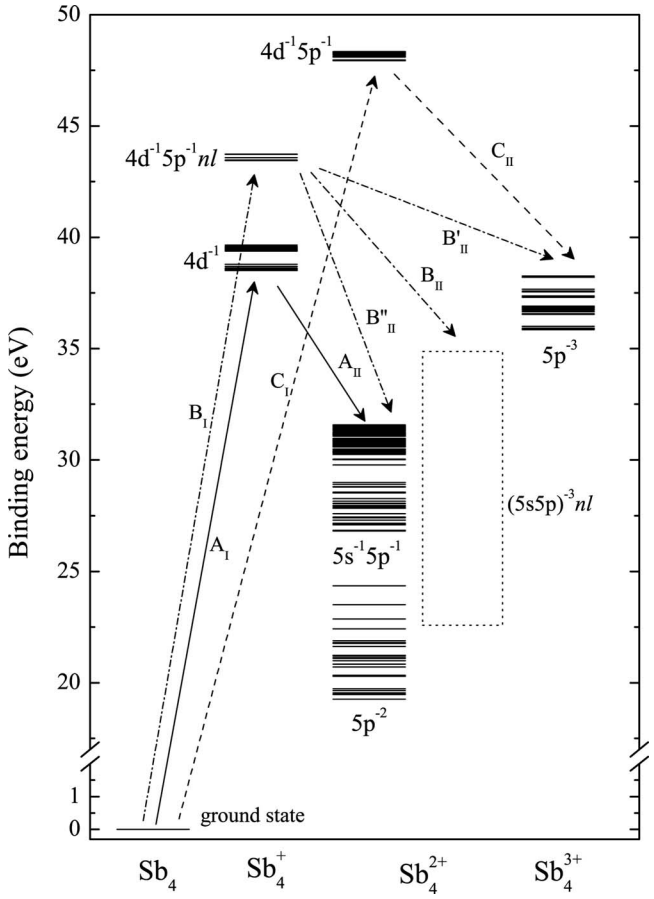

FIG. 2. Schematic energy level diagram of Sb_4. The solid lines (A_I) indicate the 4*d* ionization and the subsequent Auger decay (A_{II}). The dash-dotted lines indicate the photoionization accompanied by a shake-up transition (B_I) and the following Auger process, where the shaken electron may be a spectator in the Auger process (B_{II}), be shaken off (B'_{II}) or participate in the Auger decay (B''_{II}). The dashed lines indicate the direct double photoionization (C_I) and the following Auger decay (C_{II}). The $(5s5p)^{-3}nl$ states were placed in the diagram where they are expected to be located. No calculations for these states were performed.

bitals (MOs) $5a_1$, $6t_2$, and $2e$ are mainly linear combinations of the atomic Sb 5*p* orbitals (Fig. 1), while the inner valence $4a_1$ and $5t_2$ MOs are constructed from Sb 5*s* atomic orbitals (Fig. 1). Below the valence orbitals there are 20 Sb 4*d*-like molecular orbitals that retain most of their atomic character (Fig. 1). The lowest unoccupied MOs (LUMOs) are the $7t_2$ and $3e$, mainly of Sb 5*p* character. The most bonding orbitals of the highest occupied molecular orbitals (HOMOs) are the Sb 5*s*-type orbitals $4a_1$ and $5t_2$, of which the latter is less bonding than the former. Of the remaining Sb 5*p*-type HOMOs, the $5a_1$ and $6t_2$ present a nonbonding character and the $2e$ is an Sb-Sb bonding MO [2]. The two above-mentioned LUMOs present a clear antibonding character.

A schematic energy level diagram including the energies of the neutral and ionic states involved in transitions described in this work is shown in Fig. 2. The $4d^{-1}$, $4d^{-1}5p^{-1}nl$, and $4d^{-1}5p^{-1}$ initial ionic states are created by 90 eV photon excitation. The 4*d* hole state decays via Auger electron emission, where the outermost electrons participate

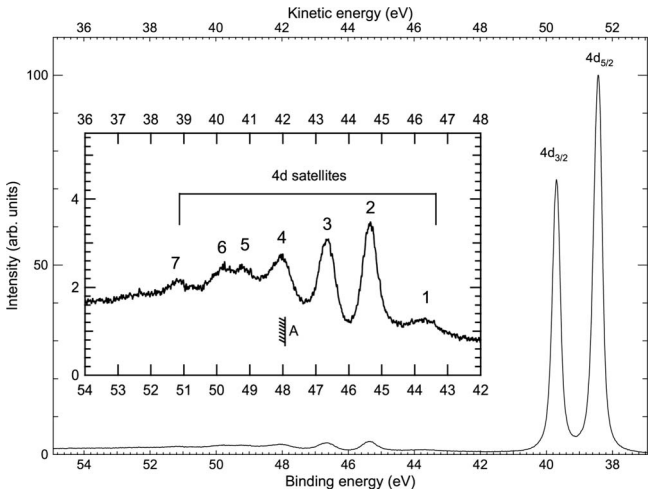

FIG. 3. Core (Sb 4*d*) photoelectron spectrum. The vertical bar *A* denotes the estimated direct double photoionization threshold. The numbers mark the shake-up satellite lines.

in the decay. For details see the figure caption and the text below.

B. The 4*d* photoelectron spectrum of Sb_4

The PES measured at the Sb_4 4*d* core shell ionization region is shown in Fig. 3. The PES is dominated by two peaks at the center binding energies of 38.51 and 39.77 eV (corresponding to transition A_I in Fig. 2). The main peaks clearly resemble the closed shell atomic structure, corresponding to the atomic Sb $4d^{-1}_{3/2,5/2}$-like states with the spin-orbit splitting of 1.26 eV, which agrees with previous experimental results from solid state antimony [9]. The intensity ratio of these two peaks was determined to be 1.42:1.00 at the photon energy of 90 eV, which is in fair agreement with the statistical population ratio of $4d_{5/2}:4d_{3/2}=1.5:1.0$.

Furthermore, at the high-binding-energy side of the 4*d* core ionization lines is the 4*d* satellite structure located above 42 eV. The binding energies of the satellite lines are presented in Table I. With the aid of the Xe 4*d* PES [10] and the molecular calculations we have been able to identify this satellite structure as the 4*d* shake-up structure (due to transitions B_I in Fig. 2), where the 4*d* core ionization is accompanied by the excitation of a valence electron from the outer-

TABLE I. The binding energies of the 4*d* satellites. The numbering of the features refers to the numbering used in Fig. 3.

Feature	Binding Energy (eV)
1	43.73
2	45.42
3	46.74
4	48.13
5	49.23
6	49.97
7	51.25

most $6t_2$ or $2e$ MOs (the $5p$-like orbitals) to lowest initially unoccupied $7t_2$ and $3e$ MOs during the photoionization. In the xenon case, the shake-up satellites are located over 14 eV above the main photolines, but in the Sb_4 cluster the lowest shake-up states were found to be only a few eV above the main lines. The series of shake-up states converge on the double photoionization threshold. The direct double ionization (transitions C_I in Fig. 2) does not produce photolines with exact energy values since the two outgoing electrons share the excess energy by an arbitrary ratio, but double photoionized states are revealed in a PES as an electron background ranging from zero kinetic energy to the double ionization threshold (vertical bar *A* in Fig. 3). The lowest doubly ionized states of Sb_4 were located at about 48 eV in the experimental spectrum.

The molecular calculations predict the energies for the main Sb $4d^{-1}$-like states to be between 42.6 and 43.7 eV and the states are located in two groups approximately 0.9 eV apart. The $4d^{-1}5p^{-1}nl$-like states are predicted to be around 52.8 eV. The calculations overestimate the binding energies by 4.1 eV as compared to the experiments. The molecular calculations predict the double ionization threshold to be at approximately 52 eV. The shake-up states are predicted to be at 0.8 eV higher in binding energies than the direct doubly ionized energy states of Sb_4, so for the shake-up states the discrepancy is larger than for the $4d^{-1}5p^{-1}$ states. It is indeed rather common—already in the case of atomic calculations—to overestimate binding energies, especially for deeply ionized states where it is very difficult to properly reproduce the relaxation effects.

C. The *NVV* Auger electron spectra of Sb_4

The AES of Sb_4 at the kinetic energy region from 5 to 22 eV measured at the photon energy of 90 eV is presented in Fig. 4. The AES consists of two transition groups, with the group located at the kinetic energies between 12 and 19 eV, showing more resolved structure than the other group at the kinetic energy region below 12 eV. In order to identify the transition groups, the ionization energies for the final ionic states having two valence holes were calculated according to Sec. III A. Calculated initial ionic states were corrected by the 4.1 eV shift due to the overestimation of the binding energies as described in Sec. III B and the kinetic energies of the Auger electrons were obtained as the difference between the initial and final state energies. According to these results, the high-kinetic-energy limit for the $(4a_1,5t_2)^{-1}(5a_1,6t_2,2e)^{-1}$ final states is at 11.82 eV (vertical bar *A* in Fig. 4 and for the $(5a_1,6t_2,2e)^{-2}$ final states at 19.56 eV (marked with vertical bar *B* in Fig. 4).

To confirm the identification of the Auger groups, based on molecular energy calculations, the intensity distribution was estimated semiempirically as follows. The peak group at higher kinetic energy can be compared to the Xe $N_{4,5}O_{2,3}O_{2,3}$ AES as the two final state holes are located on the Sb $5p$-type orbitals. The final state holes of the lower kinetic energy group are in the Sb $5s$- and Sb $5p$-type MOs, which can be compared to the Xe $N_{4,5}O_1O_{2,3}$ Auger transitions. The $N_{4,5}O_{2,3}O_{2,3}$ Auger spectrum of the Sb_4 cluster was next predicted for an isoelectronic atom. The final energy state splitting for the negative ion Sb^- with $[Kr]4d^{10}4s^25s^25p^4$ electron configuration was calculated using the nonrelativistic Cowan code [37] within the intermediate coupling scheme. The energy splitting of the five energy states relative to the lowest $^1S_0$ state were calculated to be ($^1D_2$) 1.444 eV, ($^3P_0$) 2.204 eV, ($^3P_1$) 2.270 eV, and ($^3P_2$) 2.601 eV. The $N_{4,5}O_{2,3}O_{2,3}$ Auger energies were obtained by using the experimental spin-orbit splitting of 1.26 eV for the $4d^{-1}$ initial states and shifting the semiempirical Auger group to correspond to the kinetic energies of the experimental AES. The initial state population ratio was also determined from the experimental PES (Fig. 3). The relative intensities of the Auger lines were taken from the corresponding experimental Xe $N_{4,5}O_{2,3}O_{2,3}$ AES [12]. The semiempirical $N_{4,5}O_{2,3}O_{2,3}$ AES of Sb_4 is shown in Fig. 4. The ten Auger lines were simulated by using a Voigt function with a full width at half maximum of 0.8 eV, which was defined empirically. The broadening consists of the electron energy analyzer broadening and includes the initial state broadening (250 meV from the experimental $4d$ PES). The further broadening is expected to be caused by the molecular field effects that play a more significant role in the AES as the vacancies are located in the valence shells. The semiempirical atomiclike $N_{4,5}O_{2,3}O_{2,3}$ AES fits nicely with the experimental AES of the Sb_4 cluster, which establishes that the $4d$ core hole states of Sb_4 cluster are of very atomic type and the holes in the final states of the transitions in question are in the Sb $5p$-type MOs.

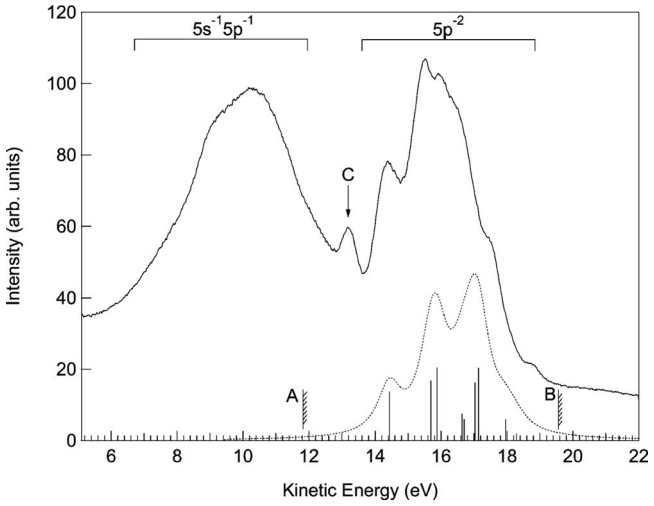

FIG. 4. *NVV* AES of Sb_4. The solid line is the experimental AES and the dashed line is the semiempirically obtained spectrum for the $5p^{-2}$-type final states. The spectra are not scaled with respect to each other. The vertical bars *A* and *B* limit the theoretical highest possible energy of final states with atomic $5s^{-1}5p^{-1}$ (11.82 eV) and $5p^{-2}$ (19.56 eV) character, respectively. The vertical sticks mark the positions and intensities of separate transitions. The arrow *C* points to a structure that was interpreted to be a part of the lines originating from the $4d^{-1}5p^{-1} \rightarrow (5s5p)^{-3}$ transitions.

The Auger spectrum to Sb $5p^{-2}$-type final states shows distinguishable peak structure while no peaks are resolved in the Auger decay spectrum to Sb $5s^{-1}5p^{-1}$-type final states. The reason for this may be the electron correlation of the $5s$-type MOs, which splits the final configuration to numer-

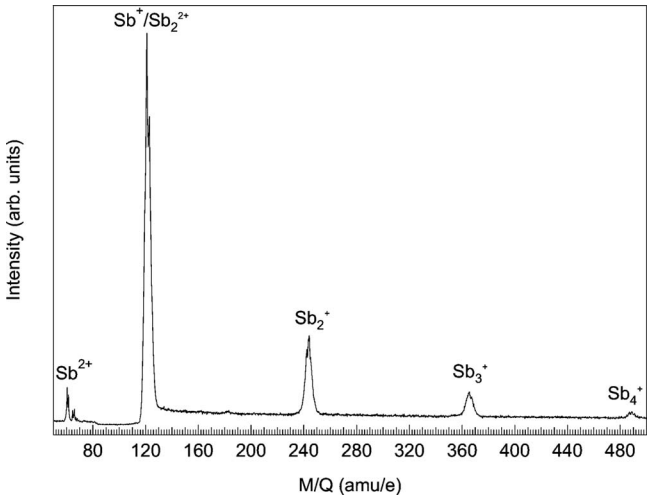

FIG. 5. Ion mass spectrum converted from a TOF spectrum recorded at 90 eV photon energy. The mass scale was calibrated using H_2O and CO_2 lines (not shown in the spectrum).

ous final states and the transition rate is distributed between all these states in similar fashion as in the $N_{4,5}O_1O_{2,3}$ AES of Xe. The electron correlation of the 5*s*-type $(4a_1, 5t_2)$ MOs is not confirmed by molecular calculations but other similarities between the 4*d* PES and subsequent AESs of Sb_4 and Xe justify this assumption.

Between the two main Auger transition groups, around the kinetic energy of 13 eV, there is a smaller peak (feature *C* in Fig. 4), which does not belong to either of the main groups. Instead, according to the molecular calculations, the kinetic energy of the structure is equal to the transition energies of the $4d^{-1}5p^{-1} \rightarrow (5s5p)^{-3}$–type satellite Auger transitions of Sb_4 (arrow C_{II} in Fig. 2). These satellite Auger transitions end up at the triply ionized states while the main Auger transitions produce doubly ionized final states. The satellite Auger transitions extend also to lower kinetic energies, but they overlap heavily with the diagram Auger transitions and are not so easily distinguished. The $N_{4,5}OO$ spectrum of Xe has the same kind of satellite structure located in between the $N_{4,5}O_1O_{2,3}$ and $N_{4,5}O_{2,3}O_{2,3}$ main Auger groups [16,17]. Also, double Auger transitions from the 4*d* shake-up states to the triply ionized final states are possible (arrow B'_{II} in Fig. 2). They are located in low kinetic energies overlapping with the $N_{4,5}O_1O_{2,3}$ main Auger group.

D. Fragmentation of Sb_4 following 4*d* photoionization and subsequent Auger decay

1. Ion TOF spectrum

In Fig. 5 the ion mass spectrum of Sb_4 measured at the ionizing photon energy of 90 eV is presented. Antimony has two naturally occurring isotopes with atomic masses of 120.9 and 122.9 a.m.u. The natural abundances of these isotopes are 57.21% and 42.79%, respectively. The isotope splitting can be clearly seen in the mass peak corresponding to Sb^+ and Sb^{2+} ions. Also the intensity ratio of the two peaks in the Sb^{2+} signal (1.3:1) is in line with the natural abundance ratio of 1.3:1. Similar behavior is seen in the Sb_2^+ peak, where three types of isotope combinations are possible. However, the dip between the peaks in Sb^+ is less pronounced than the one between the Sb^{2+} peaks. This indicates that some Sb_2^{2+} is also present as the Sb_2^{2+} ion can be identified as a peak arising from a combination of the two isotopes between the two Sb^+ peaks. On the other hand, the unstable doubly charged dimer can fragment before detection via Coulomb explosion into Sb^+ ions also overlapping the Sb^+ signal. However, the presence of the doubly charged dimer in the TOF spectrum can be explained by metastable states of Sb_2^{2+}, which are long enough lived to make observation of the fragment possible. Furthermore, this species has been previously observed experimentally by Umemura *et al.* [18], indicating that some of the fragments can be observed before further dissociation takes place. The other observed fragments are the Sb_3^+ and Sb_4^+ ions, which are seen as even broader structures due to a large number of isotope combinations.

TABLE II. The kinetic energy ranges for the electron-ion coincidence maps and the numbering of the regions.

Region number	E_k^{start} (eV)	E_k^{end} (eV)	Comment
1	48	54	4*d* main
2	37	48	4*d* satellites
3	16	22	Auger
4	11	17	Auger
5	6	12	Auger

2. Electron-ion coincidences

The coincidence data were collected in five separate regions: The photoelectron spectrum was divided into the 4*d* main photoline region and the satellite line region. The coincidence events from the Auger electrons were measured in three slightly overlapping regions. The numbering of the regions with their respective kinetic energy ranges is presented in Table II. The obtained photoelectron-photoion coincidence (PEPICO) maps are presented in Fig. 6 and the Auger electron-ion coincidence maps are presented in Fig. 7.

It can be seen in both Figs. 6 and 7 that no Sb_4^+ ions are present following the 4*d* core ionization. This means that the cluster is always fragmented after core ionization and the following electronic decay. The observation of Sb_4^+ ions in the TOF spectrum measured at 90 eV photon energy (see Fig. 5) can be explained by the direct ionization of the valence orbitals. The tendency of clusters with a single vacancy in the valence states to fragment is obviously not as strong.

The largest ion detected is Sb_3^+, which is created only in coincidence with the main photoelectrons (region 1) and Auger electrons corresponding to Sb $5p^{-2}$ type of final states (regions 3 and 4). In the case of $5p^{-2}$-type states the electrons spend little time between the four atoms as the $5a_1$ and $5t_2$ MOs are nonbonding in character and the $2e$ MOs correspond to Sb-Sb bonding. The 5*s*-type electrons on the $4a_1$ MOs are, on the other hand, tightly shared by all of the atoms in the cluster (see Fig. 1) corresponding to strong bonding effects. This is also true for the $5t_2$ MOs although

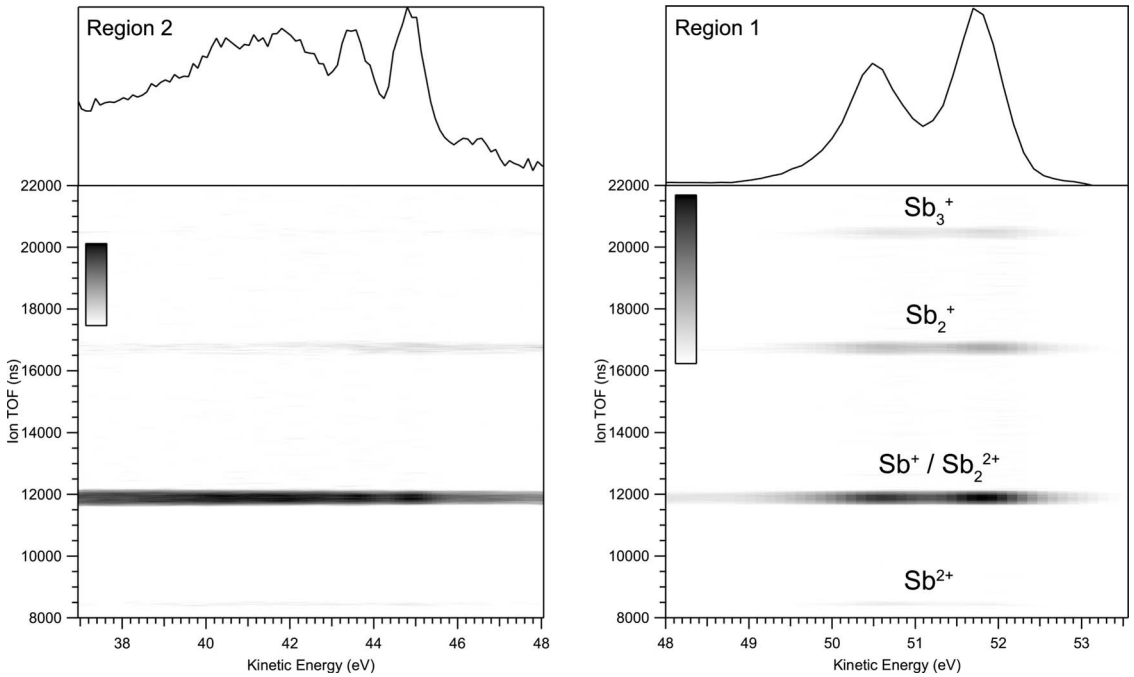

FIG. 6. PEPICO map of the satellite lines (region 2) and 4*d* main photolines (region 1). The intensity scale of the electron spectrum of the satellite lines is magnified by a factor of 30 with respect to the main photolines.

the bonding is somewhat weaker than that for the $4a_1$ MOs. Thus the removal of the electrons from the totally symmetric bonding $4a_1$ orbital ($5s^{-1}5p^{-1}$-type states in region 5) is likely to favor complete atomization of the cluster. Ionization of outer valence orbitals leaves some Sb-Sb bonds unaffected and thus enhances the probability of producing heavier fragments. The next largest and second most abundant fragment observed is the Sb_2^+ ion. It is detected in coincidence with both the main photolines and the satellite lines as well as with both of the Auger transition groups (regions 3 and 4). This fragment is not observed in region 5 below the electron kinetic energy of 9 eV. These electrons correspond to $5s^{-2}$ and $5p^{-3}$ final states which are highly dissociative in nature. Also the $(5s5p)^{-3}nl$-type final states are located at these energies, having highly dissociative character due to the 5*s* hole and shake-up to a strongly antibonding LUMO.

The most abundant ion observed in all of the regions is the Sb^+ ion, but the signal is overlapped by the Sb_2^{2+}, which has the same mass to charge ratio and thus the same flight time as the Sb^+ ion.

The fastest ion detected is the doubly charged Sb^{2+}. The signal is very weak, but it can be observed in coincidence with both the main photoelectron lines and the satellite lines as well as in all three Auger regions. The existence of a

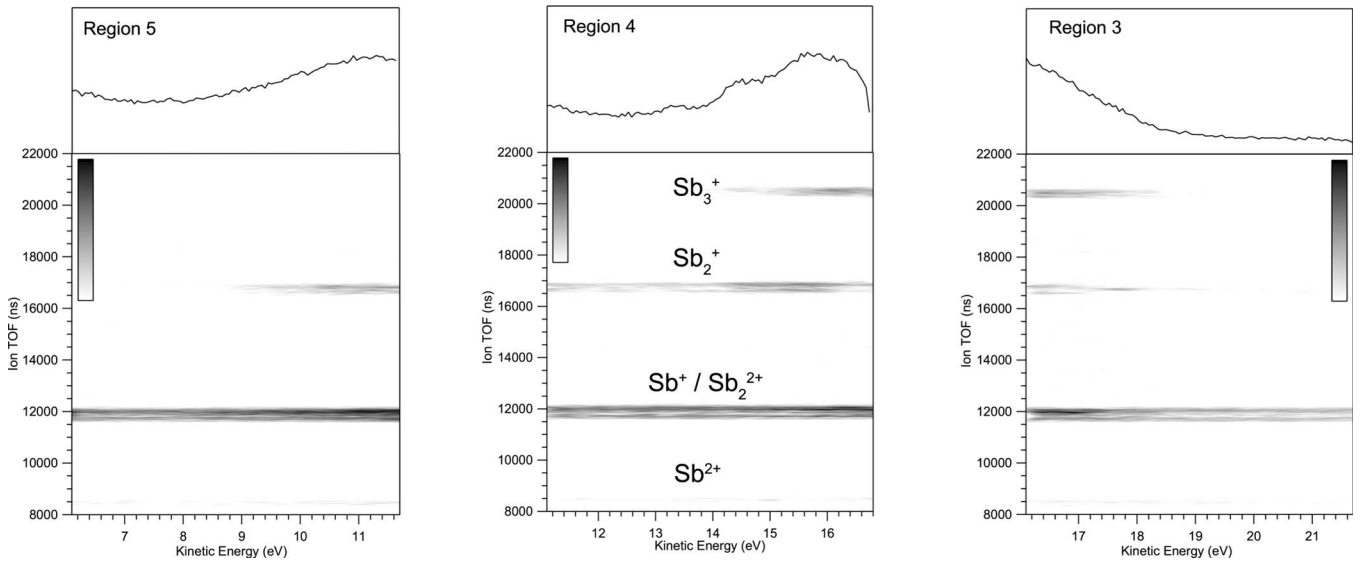

FIG. 7. Electron-ion coincidence map of the Auger electrons. All spectra are presented at the same intensity scale.

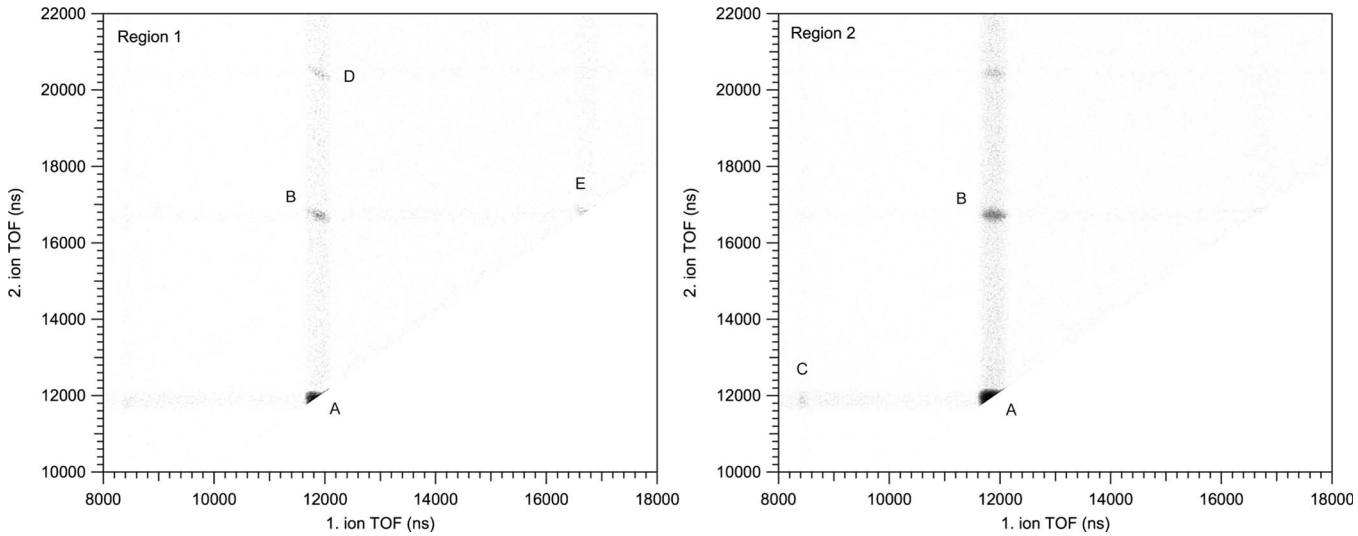

FIG. 8. Ion-ion coincidence maps of the photoelectrons and satellites. The labels correspond to ion pairs as presented in Table III.

doubly charged fragment in the region of main photolines means that it must originate from the Auger decay. This is the only possible fragmentation pathway as cascade Auger transitions from the $5s^{-1}5p^{-1}$- or $5p^{-2}$-type states to the $(5s5p)^{-3}$-type states are energetically impossible (see Fig. 2). The same reasoning can be used also in the satellite region, but also the direct double photoionization to $4d^{-1}5p^{-1}$-type states contributes to the creation of Sb^{2+}. This doubly ionized state can then further decay to the $(5s5p)^{-3}$-type states via Auger transition and thus a triply charged group of clusters must exist. Indeed in the ion-ion coincidence spectra (see Sec. III D 3) a coincidence of Sb^{2+} and Sb^{+} can be observed in the satellite region and the Auger regions. The direct double photoionization channel also results in a constant background in the coincidence maps from the double ionization threshold to zero kinetic energy, which explains the weak constant Sb^{2+} signal observed in all three Auger regions.

The fact that the Sb^{+}-$Sb_2{}^{2+}$ signal extends also throughout the whole measurement region—and especially to the very low-kinetic-energy region below the $5s^{-1}5p^{-1}$-type states—can be interpreted so that a large part of the signal is due to the direct double photoionization fragmenting the cluster into $Sb_2{}^{2+}$ ions and neutral Sb_2. This assumption is further justified by the measured ion-ion coincidences (see Sec. III D 3).

3. Ion-ion coincidences

In order to study experimentally the fragmentation pathways leading to the ionized products observed the electron-ion-ion coincidence technique has been employed. The electron-ion-ion coincidence maps are shown in Fig. 8 for the photoelectrons and in Fig. 9 for the Auger electrons. Studying the electron-ion-ion coincidence maps of all the experimental regions, several fragmentation pathways can be found for the different ion pairs. The observed ion-ion coincidences are listed and labeled in Table III. The signal of event *C* is very weak, but it shows that also some triply ionized Sb_4 is present, which in turn indicates either a second-step Auger decay or a direct double photoionization followed by the emission of an Auger electron. The fact that event *C* is not observed together with the 4*d* main photoelectrons is well in line with the earlier conclusion that no cascade processes from the doubly charged final states are possible. Thus for the triply ionized final states the only available channel is the one with initial double photoionization (C_{I} in Fig. 2) and subsequent Auger decay (C_{II} in Fig. 2).

The ion-ion pairs can be a product of several kinds of dissociation process. In the case of a doubly charged final state the two-body and three-body reactions are considered. In two-body dissociation (TD) the cluster is directly split into two singly charged particles, whereas in the three-body reaction a third neutral particle is emitted. These three-body reactions can be further divided into three kinds of process called *deferred charge separation* (DCS), *secondary dissociation* (SD), and *concerted dissociation* (CD). In DCS the neutral fragment is emitted first and the fragmentation into two charged particles follows. In SD the two singly charged fragments are first formed, after which one of them emits a neutral particle. In CD all fragments are emitted simultaneously, and the momentum correlation between the two ions detected is lost. The type of fragmentation can be extracted from the shape or slope of the coincidence event in the ion-ion coincidence map, which possesses the information about the momentum correlation between the emitted fragments [38,39]. In the case of a triply charged final state four-body fragmentations are also possible. These, however, are not considered in the present study.

The experimental slopes of the coincidence pattern were determined by a coordinate system transformation. First the two flight time axes were rotated and then the coincidence pattern was projected onto the *x* axis. The projection was fitted using a Gaussian function. Then the slope was calculated from the rotation angle that gave the narrowest projection, assuming that in this case the coincidence pattern was vertically oriented and the flight time spread due to correlated two-ion Coulomb explosion was eliminated. The results of fitting and the corresponding fragmentation mechanisms

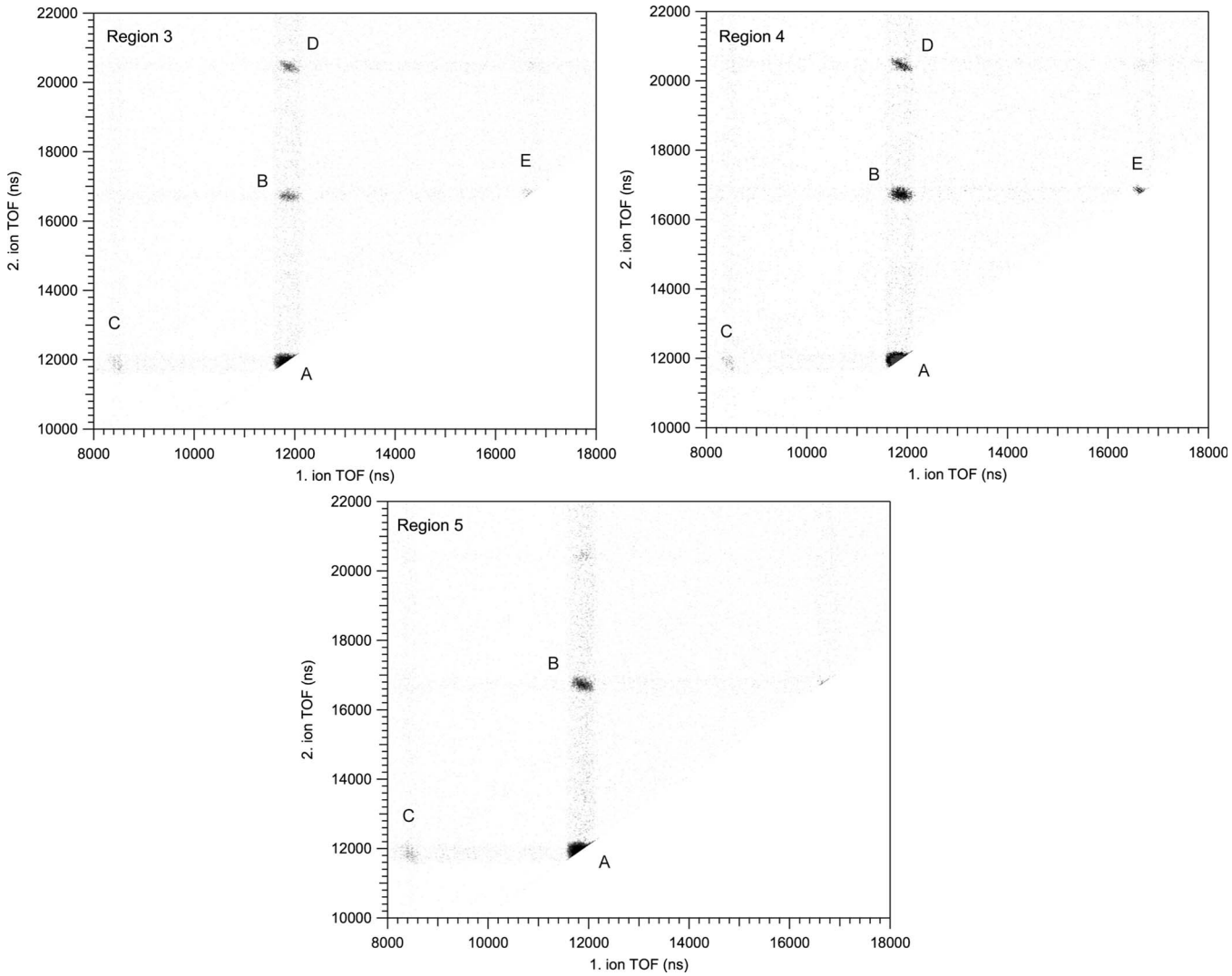

FIG. 9. Ion-ion coincidence maps of the Auger electrons. The labels correspond to ion pairs as presented in Table III.

are presented in Table IV. The determination of the slopes was hindered by the several isotope combinations that broaden and scramble the events in the coincidence maps. Also, the possibility of four-body fragmentations, where ion-ion-ion coincidence techniques should be employed, destroys the momentum correlation between the fragments and could cause significant smearing of the coincidence events. All these effects reflect in the rather large error limits for the determined slopes.

TABLE III. The observed ion-ion-coincidence events and theoretical slopes for possible fragmentation pathways. For the event *A* the pathways are too numerous to list the possible slopes here.

Event	Ion pair	Slope(s)
A	$Sb^+ + Sb^+$	
	$Sb_2^{2+} + Sb^+$	
B	$Sb^+ + Sb_2^+$	−0.67, −1, −1.5, −2
C	$Sb^{2+} + Sb^+$	−1.5, −2, −6
D	$Sb^+ + Sb_3^+$	−1
E	$Sb_2^+ + Sb_2^+$	−1

The events *D* and *E* are trivial in the sense that no neutral fragment can be emitted. The slope of these events from the electron-ion-ion coincidence maps has been determined to be very close to −1. It should be noted that the event *D* exists only in the regions 1, 3, and 4. This is in line with the fact that the 5*s*-type orbitals are more bonding in character than the 5*p*-type orbitals (see Sec. III D 2). The same reasoning applies for the $Sb_2^+ + Sb_2^+$ coincidence event.

For the event *A* many fragmentation pathways with all possible mechanisms leading to the same end products exist and the event in the coincidence map consists of many overlapping features with different slopes that are not distinguishable from one another. Characterization of this event is further complicated by the fact that coincidences involving both the Sb_2^{2+} and Sb^+ fragments as well as the $Sb^+ + Sb^+$ coincidences following the Coulomb explosion of the doubly charged dimer are also spread over the same area. This is seen as a growth of the area covered by the coincidence

TABLE IV. The slopes of the coincidence events determined using the method described in the text with their error limits and corresponding fragmentation mechanisms. The question marks indicate that the values could not be determined. The dash tells that the event in question was not observed in the region.

	Slope					Error					Mechanism				
	1	2	3	4	5	1	2	3	4	5	1	2	3	4	5
A								?							
B	−0.8	−0.5	−0.4	−1.0	−1.0	±0.3	±0.2	±0.2	±0.4	±0.4	DCS	SD	SD	DCS	DCS
				−2					±0.8					SD	
C	—	−2.7	−2.2		?	—	±1.0	±0.9		?	—	SD	SD		?
				−4.7					±1.6					DCS	
D	−1.0	—	−1.0	−0.9	—	±0.2	—	±0.3	±0.2	—	TD	—	TD	TD	—
E	−1.0	—	−1.0	−1.0	—	?	—	?	?	—	TD	—	TD	TD	—

events in the ion-ion coincidence maps, when such coincidences are possible. Indeed the area covered by the $Sb^+ + Sb^+$ events in coincidence with the 4*d* main photoelectrons is much smaller than the respective area in all other regions. This can be explained by the fact that overlapping $Sb^+ + Sb_2^{2+}$ coincidences become possible only after the direct double photoionization, that can result in triply charged final states.

When studying the ion pair *B* some notable differences can be seen at different measurement regions. In the region 1 of the 4*d* main photolines the slope of the event is very close to −1 and thus a deferred charge separation takes place:

$$Sb_4^{2+} \rightarrow Sb_3^{2+} + Sb,$$

$$Sb_3^{2+} \rightarrow Sb^+ + Sb_2^+. \quad (2)$$

The fragmentation pathway is different, when looking at the ions in coincidence with the 4*d* satellite photolines, since here the slope of the event is very close to −0.5. This indicates a secondary dissociation with the following (theoretical slope −0.67) mechanism

$$Sb_4^{2+} \rightarrow Sb^+ + Sb_3^+,$$

$$Sb_3^+ \rightarrow Sb_2^+ + Sb. \quad (3)$$

In the Auger regions 3–5 both mechanisms are observed so that in region 3 the slope is close to −0.5 and in regions 4 and 5 the slope is −1. In principle the ion pair $Sb_2^{2+} + Sb_2^+$ could also exist in the same position with a slope of −2, but no such events were observed.

The ion pair *C* is not observed in coincidence with the 4*d* main photoelectrons, but a weak signal is present in the satellite region. This is again in line with the fact that the triply ionized Sb_4 is created after Auger decay following direct double photoionization. A double ion yield (DIY) spectrum of the ion pair *C* is presented in Fig. 10. The DIY spectrum shows the amount of events in which both of the selected ions are observed as a function of the emitted electron energy. It can be clearly seen that the ion pair production peaks between 12 and 14.5 eV. This is an experimental verification for the theoretical prediction that feature *C* in Fig. 4 originates from the $4d^{-1}5p^{-1} \rightarrow (5s5p)^{-3}$ transitions.

The ion pair *C* is observed in all three Auger regions. In this process a neutral fragment is emitted and the following three mechanisms are possible:

$$Sb_4^{3+} \rightarrow Sb_3^{2+} + Sb^+,$$

$$Sb_3^{2+} \rightarrow Sb^{2+} + Sb, \quad (4)$$

$$Sb_4^{3+} \rightarrow Sb_3^+ + Sb^{2+}$$

$$Sb_3^+ \rightarrow Sb^+ + Sb_2, \quad (5)$$

$$Sb_4^{3+} \rightarrow Sb_2^{3+} + Sb_2$$

$$Sb_2^{3+} \rightarrow Sb^{2+} + Sb^+. \quad (6)$$

The theoretical slopes for these processes are −1.5, −6, and −2, respectively. Of these −6 can be found in region 4. The other two are more difficult to distinguish from each other, but it seems that the slope with −2 is more dominating

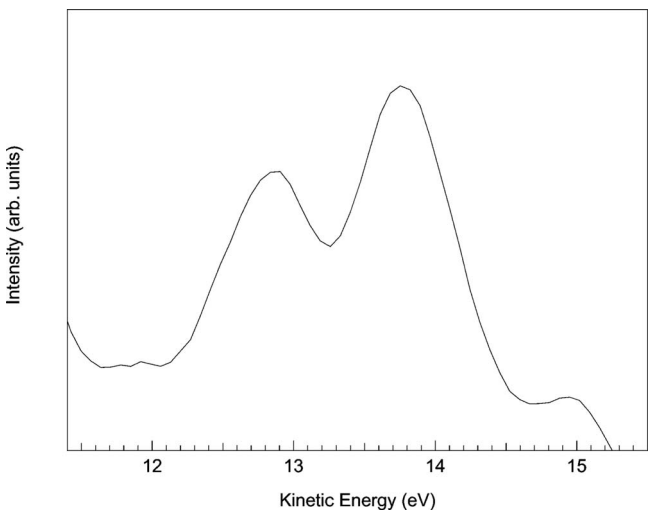

FIG. 10. DIY spectrum of ion pair *C* as a function of emitted electron energy. The intensity has been normalized to the electron counts to normalize the rate of uncorrelated ions to constant level. The spectrum has been smoothed in order to reduce the noise level.

although the −1.5 falls within the error limits in many regions. This indicates that in the fragmentation of triply charged Sb_4 SD is the favored pathway.

IV. CONCLUSIONS

The molecular calculations combined with the described semiempirical method using negative ion atomic calculations and existing experimental data of Xe provide a useful tool in identifying the transitions observed in the experimental PES and AES of Sb_4. These methods allowed the identification of the two large peak groups in the AES as well as predicted the existence of lines originating from the Auger decay following the direct double photoionization between the large peak groups.

The ion TOF, electron-ion, and electron-ion-ion coincidence techniques serve as very useful tools in further assigning the electron spectra, when the bonding properties of the orbitals taking part in the transitions are known. The electron-ion coincidence methods allowed us to study also the fragmentation of the Sb_4 clusters, and the experimental results are well in line with the theoretically modeled bonding properties of the MOs, where the electron vacancies are created. The electron-ion-ion coincidence techniques provided more detailed information about the fragmentation pathways of the cluster. The combinations of the two naturally occurring isotopes in the Sb_4 clusters overlap heavily in the ion TOF spectra as well as in the coincidence maps. This causes problems in determining the accurate slopes of the ion-ion coincidence events, thus making it more difficult to distinguish all possible fragmentation pathways.

In order to reliably theoretically verify and study the physical origins of the observed favored fragmentation pathways the potential energy hypersurfaces of the doubly and triply ionized Sb tetramer and the fragmentation products should be studied in detail. This rather complicated work, however, is left for the future. More experimental information on the fragmentation of the triply ionized clusters could also be gained by employing electron-ion-ion-ion coincidence techniques.

ACKNOWLEDGMENTS

This work has been financially supported by the Research Council for Natural Sciences of the Academy of Finland and the European Community Research Infrastructure Action under the FP6 "Structuring the European Research Area" Program (through the Integrated Infrastructure Initiative "Integrating Activity on Synchrotron and Free Electron Laser Science"). S.U., M.H., and A.C. would like to thank Vilho, Yrjö, and Kalle Väisälä Foundation and S.U. the Tauno Tönning Foundation for financial support. We thank Dr. Rami Sankari for the preparatory work. We acknowledge the staff of MAX-lab for their assistance during the experiments.

[1] K. Sattler, J. Mühlbach, and E. Recknagel, Phys. Rev. Lett. **45**, 821 (1980).
[2] S. Elbel, J. Kudnig, M. Grodzicki, and H. J. Lempka, Chem. Phys. Lett. **109**, 312 (1984).
[3] L. S. Wang, Y. T. Lee, D. A. Shirely, K. Balasubramanian, and P. Feng, J. Chem. Phys. **93**, 6310 (1990).
[4] L. S. Wang, B. Niu, Y. T. Lee, D. A. Shirley, E. Ghelichkhani, and E. R. Grant, J. Chem. Phys. **93**, 6318 (1990).
[5] L. S. Wang, B. Niu, Y. T. Lee, D. A. Shirley, E. Ghelichkhani, and E. R. Grant, J. Chem. Phys. **93**, 6327 (1990).
[6] V. Kumar, Phys. Rev. B **48**, 8470 (1993).
[7] H. Aksela, J. Väyrynen, and S. Aksela, J. Electron Spectrosc. Relat. Phenom. **16**, 339 (1979).
[8] C. Bréchignac, M. Broyer, Ph. Cahuzac, M. de Frutos, P. Labastie, and J.-Ph. Roux, Phys. Rev. Lett. **67**, 1222 (1991).
[9] R. A. Pollak, S. Kowalczyk, L. Ley, and D. A. Shirley, Phys. Rev. Lett. **29**, 274 (1972).
[10] S. Svensson, B. Eriksson, N. Mrtensson, G. Wendin, and U. Gelius, J. Electron Spectrosc. Relat. Phenom. **47**, 327 (1988).
[11] T. X. Carroll, J. D. Bozek, E. Kukk, V. Myrseth, L. J. Saethre, T. D. Thomas, and K. Wiesner, J. Electron Spectrosc. Relat. Phenom. **125**, 127 (2002).
[12] A. Kivimäki, L. Pfeiffer, H. Aksela, E. Nõmmiste, and S. Aksela, J. Electron Spectrosc. Relat. Phenom. **101-103**, 43 (1999).
[13] J. Jauhiainen, H. Aksela, S. Aksela, A. Kivimäki, O.-P. Sairanen, E. Nõmmiste, and J. Vgh, J. Phys. B **28**, 3831 (1995).
[14] S. Alitalo, A. Kivimäki, T. Matila, K. Vaarala, H. Aksela, and S. Aksela, J. Electron Spectrosc. Relat. Phenom. **114-116**, 141 (2001).
[15] T. Hayaishi, E. Murakami, Y. Morioka, H. Aksela, S. Aksela, E. Shigemasa, and A. Yagishita, Phys. Rev. A **44**, R2771 (1991).
[16] A. Kivimäki, H. Aksela, J. Jauhiainen, A. Naves de Brito, O.-P. Sairanen, S. Aksela, A. Ausmees, S. J. Osborne, and S. Svensson, Phys. Rev. A **49**, 5124 (1994).
[17] L. Partanen, M. Huttula, S. Heinäsmäki, H. Aksela, and S. Aksela, J. Phys. B **40**, 4605 (2007).
[18] K. Umemura, Y. Kawanami, and T. Ishitani, Jpn. J. Appl. Phys., Part 2 **27**, L2392 (1988).
[19] E. Rühl, Int. J. Mass. Spectrom. **229**, 117 (2003).
[20] A. F. Lago, A. C. F. Santos, and G. G. B. de Souza, J. Chem. Phys. **120**, 9547 (2004).
[21] A. C. F. Santos, C. A. Lucas, and G. G. B. de Souza, Chem. Phys. **282**, 315 (2002).
[22] M. Simon, M. Lavollée, M. Meyer, and P. Morin, J. Electron Spectrosc. Relat. Phenom. **79**, 401 (1996).
[23] E. Kukk, G. Prümper, R. Sankari, M. Hoshino, C. Makochekanwa, M. Kitajima, H. Tanaka, H. Yoshida, Y. Tamenori, E. Rachlew, and K. Ueda, J. Phys. B **40**, 3677 (2007).
[24] M. Bässler, A. Ausmees, M. Jurvansuu, R. Feifel, J.-O. Forsell, P. de Tarso Fronseca, A. Kivimäki, S. Sundin, and S. L. Sorensen, Nucl. Instrum. Methods Phys. Res. A **469**, 382 (2001).
[25] M. Huttula, M. Harkoma, E. Nõmmiste, and S. Aksela, Nucl. Instrum. Methods Phys. Res. A **467**, 1514 (2001).
[26] M. Huttula, S. Heinäsmäki, H. Aksela, E. Kukk, and S. Aksela,

J. Electron Spectrosc. Relat. Phenom. **156-158**, 270 (2007).
[27] E. Kukk, R. Sankari, M. Huttula, A. Sankari, H. Aksela, and S. Aksela, J. Electron Spectrosc. Relat. Phenom. **155**, 141 (2007).
[28] R. E. Honig and D. A. Kramer, RCA Rev. **30**, 285 (1969).
[29] M. Huttula *et al.* (unpublished).
[30] M. Jurvansuu, A. Kivimäki, and S. Aksela, Phys. Rev. A **64**, 012502 (2001).
[31] H. Aksela, S. Aksela, and H. Pulkkinen, Phys. Rev. A **30**, 2456 (1984).
[32] M. W. Schmidt *et al.*, J. Comput. Chem. **14**, 1347 (1993).
[33] M. S. Gordon and M. W. Schmidt, in *Theory and Applications of Computational Chemistry: The First Forty Years*, edited by C. E. Dykstra, G. Frenking, K. S. Kim, and G. E. Scuseria (Elsevier, Amsterdam, 2005).
[34] J. Ivanic, J. Chem. Phys. **119**, 9364 (2003).
[35] J. Ivanic, J. Chem. Phys. **119**, 9377 (2003).
[36] L. A. LaJohn, P. A. Christiansen, R. B. Ross, T. Atashroo, and W. C. Ermler, J. Chem. Phys. **87**, 2812 (1987).
[37] R. D. Cowan, *The Theory of Atomic Structure and Spectra* (University of California Press, Berkeley, 1981).
[38] J. H. D. Eland, Acc. Chem. Res. **22**, 381 (1989).
[39] M. Simon, T. Lebrun, R. Martins, G. G. B. de Souza, I. Nenner, M. Lavolée, and P. Morin, J. Phys. Chem. **97**, 5228 (1993).